World Academy of Science, Engineering and Technology
International Journal of Mechanical and Mechatronics Engineering
Vol:12, No:5, 2018

Study on Sharp V-Notch Problem under Dynamic Loading Condition Using Symplectic Analytical Singular Element

Xiaofei Hu, Zhiyu Cai, Weian Yao

***Abstract*—**V-notch problem under dynamic loading condition is considered in this paper. In the time domain, the precise time domain expanding algorithm is employed, in which a self-adaptive technique is carried out to improve computing accuracy. By expanding variables in each time interval, the recursive finite element formulas are derived. In the space domain, a Symplectic Analytical Singular Element (SASE) for V-notch problem is constructed addressing the stress singularity of the notch tip. Combining with the conventional finite elements, the proposed SASE can be used to solve the dynamic stress intensity factors (DSIFs) in a simple way. Numerical results show that the proposed SASE for V-notch problem subjected to dynamic loading condition is effective and efficient.

***Keywords*—**V-notch, dynamic stress intensity factor, finite element method, precise time domain expanding algorithm

I. Introduction

SHARP V-notch subjected to dynamic loading condition can be found in many engineering applications. Due to the stress concentration in the vicinity of the notch tip, the initiation of cracks is likely to occur and further result in the structural failure or shorten the service life. Consequently, an accurate evaluation of the stress distribution around the V-notch tip is of significant importance for a reliable performance analysis of the structures containing V-notches. And it is necessary to investigate the fracture mechanics parameters at the notch tip, e.g., the DSIFs.

The sharp V-notch problem has been studied by using different numerical methods, including the boundary element method (BEM) [1], the finite element method (FEM) [2], the fractal-like FEM (FFEM) [3], the body force method (BFM) [4], the boundary collocation method (BCM) [5] and the extended finite element method (XFEM) [6]. Among them, FEM is the most commonly used numerical method in recent years. As a matter of fact, complex post-processing should be carried out to get the DSIFs of the V-notch.

In the previous studies, Yao and Hu proposed a novel SASE for various crack problems [7], [8]. It was demonstrated that the numerical results are precise and stable with the change of the element size and the number of nodes. In fact, the SASE can also deal with the V-notch problems. However, the existing studies were concerned on static or quasi-static problems, dynamic problem has not been considered.

In this study, the precise time domain expanding algorithm proposed by Yang [9] is used for the discretization of the time domain due to its advantages. In the space domain, the SASE which is constructed by using the analytical eigenexpanding terms is used to address the stress singularity in the vicinity of the V-notch tip, while the other area is meshed by conventional elements. The numerical solutions of the DSIFs are directly calculated through the relationship between the DSIFs and the expanding coefficients of the eigenexpansion, without any post-processing. Numerical examples are conducted, and the results show that the proposed method is effective and efficient.

II. Governing Equations

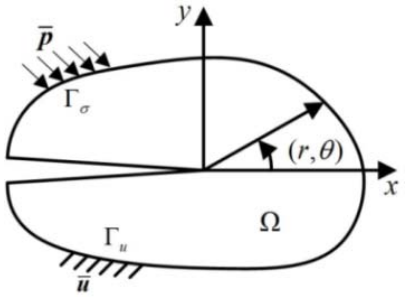

Fig. 1 A two dimensional (2D) dynamic V-notch problem

The fundamental equations for 2D dynamic problem can be given as follows: The differential equation of motion

$$\boldsymbol{L}^{\mathrm{T}}\boldsymbol{\sigma} - \rho\frac{\partial^2 \boldsymbol{u}}{\partial t^2} + \boldsymbol{f} = \boldsymbol{0},\ 0 \le t < \infty,\ (x,y) \in \Omega \tag{1}$$

The relationship between stress and strain

$$\boldsymbol{\sigma} = \boldsymbol{D}\boldsymbol{\varepsilon} \tag{2}$$

The relationship between displacement and strain

$$\boldsymbol{\varepsilon} = \boldsymbol{L}\boldsymbol{u} \tag{3}$$

The boundary conditions can be specified by

$$\boldsymbol{u} = \bar{\boldsymbol{u}} \ \text{ on } \Gamma_u \tag{4}$$

Xiaofei Hu is with the State Key Laboratory of Structural Analysis for Industrial Equipment, International Research Center for Computational Mechanics, Dalian University of Technology, Dalian, 116024, P. R. China (e-mail: hxf@dlut.edu.cn).

$$\boldsymbol{p} = \bar{\boldsymbol{p}} \ \text{on}\ \Gamma_\sigma \tag{5}$$

The initial conditions of the whole domain can be given by

$$\boldsymbol{u} = \boldsymbol{u}_0,\ \frac{\partial \boldsymbol{u}}{\partial t} = \dot{\boldsymbol{u}}_0,\ t = 0,\ (x, y) \in \Omega \tag{6}$$

In the precise time-domain expanding algorithm, the time domain is divided into a number of time intervals. In each time interval, all the time-related variables can be expanded by the dimensionless parameter s, which is specified as

$$s = (t - t_0)/T,\ \ t_0 \le t \le t_0 + T \tag{7}$$

where t_0 and T are the initial point and the size, respectively. Thus $\boldsymbol{u}$, $\boldsymbol{\sigma}$, $\boldsymbol{\varepsilon}$, $\boldsymbol{f}$ and $\boldsymbol{p}$ can be expanded in the following forms

$$\begin{aligned} &\boldsymbol{u} = \sum_{m=0} \boldsymbol{u}^m s^m, \boldsymbol{\sigma} = \sum_{m=0} \boldsymbol{\sigma}^m s^m,\ \boldsymbol{\varepsilon} = \sum_{m=0} \boldsymbol{\varepsilon}^m s^m, \\ &\boldsymbol{f} = \sum_{m=0} \boldsymbol{f}^m s^m, \boldsymbol{p} = \sum_{m=0} \boldsymbol{p}^m s^m \end{aligned} \tag{8}$$

where the non-negative integer $m = 0, 1, 2, \ldots$ is the expanding order index. Similarly, the prescribed boundary conditions can also be expanded as

$$\bar{\boldsymbol{u}} = \sum_{m=0} \bar{\boldsymbol{u}}^m s^m \ \text{on}\ \Gamma_u \tag{9}$$

$$\bar{\boldsymbol{p}} = \sum_{m=0} \bar{\boldsymbol{p}}^m s^m \ \text{on}\ \Gamma_\sigma \tag{10}$$

The first and second order derivatives of the displacement with respect to time coordinate can be given by

$$\frac{\partial \boldsymbol{u}}{\partial t} = \sum_{m=0} \frac{m+1}{T} \boldsymbol{u}^{m+1} s^m,\ \frac{\partial^2 \boldsymbol{u}}{\partial t^2} = \sum_{m=0} \frac{(m+1)(m+2)}{T^2} \boldsymbol{u}^{m+2} s^m \tag{11}$$

Through (8)-(11), the fundamental equations and boundary conditions can be rewritten using the recursive form. The explicit expressions are given as follows:

The fundamental equations

$$\boldsymbol{L}^{\mathrm{T}} \boldsymbol{\sigma}^m - \frac{(m+1)(m+2)}{T^2} \rho \boldsymbol{u}^{m+2} + \boldsymbol{f}^m = \boldsymbol{0} \tag{12}$$

$$\boldsymbol{\sigma}^m = \boldsymbol{D} \boldsymbol{\varepsilon}^m \tag{13}$$

$$\boldsymbol{\varepsilon}^m = \boldsymbol{L} \boldsymbol{u}^m \tag{14}$$

The boundary conditions

$$\boldsymbol{u}^m = \bar{\boldsymbol{u}}^m \ \text{on}\ \Gamma_u \tag{15}$$

$$\boldsymbol{p}^m = \bar{\boldsymbol{p}}^m \ \text{on}\ \Gamma_\sigma \tag{16}$$

III. Symplectic Analytical Singular Element

A sector element (SASE) with radius R is constructed in polar coordinate system, to represent the vicinity of the crack tip. As shown in Fig. 2, there are N nodes uniformly distributed on the element's boundary. They are used to connect the outside regular elements directly, and each of them has two degrees of freedom.

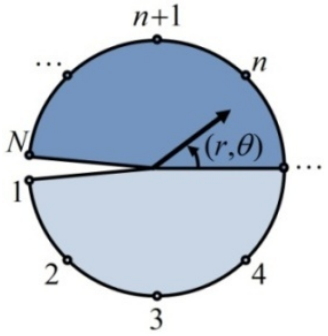

Fig. 2 The illustration of the SASE

The solution for static problem can be given in the form of eigenexpansion as follows

$$\{u_r \quad u_\theta \quad r\sigma_r \quad r\sigma_{r\theta}\} = \sum_{i=0}^{\infty} a_i^m r^{\mu_i} \psi_i(\theta) \tag{17}$$

where μ_i and ψ_i denote the eigenvalues and the corresponding eigenvectors, respectively. a_j^m is the unknown eigenexpanding coefficients to be solved. It should be noted that all the eigenexpanding terms are arranged in an ascending order according to the values of eigenvalues. It may be noted that the eigensolution for V-notch problem is different from crack problem and can be found in existing literatures [10]. Thus, the displacement field around the crack tip can be defined by using (17), as specified by

$$\boldsymbol{u}_p^m(r, \theta) = \sum_{i=0}^{\infty} a_i^m r^{\mu_i} \psi_{\boldsymbol{u},i}(\theta) \tag{18}$$

where $\boldsymbol{u}_p^m = \{u_r \quad u_\theta\}^{\mathrm{T}}$ is the vector of displacements under polar coordinates.

Although the eigensolution used in (18) cannot strictly satisfy the governing equations of dynamic problem, the displacement and stress fields defined by it are still close to the analytical solution. Therefore, it can bring many advantages to use (18) to represent the vicinity of the crack tip, instead of conventional shape functions.

In practical usage, the number of expanding terms of (18) should be finite. The first $2N$ terms are used. Thus, (18) can be given by

$$\boldsymbol{u}_p^m = \boldsymbol{\phi}_u^{\mathrm{T}}(\theta)\mathrm{diag}(r^{\mu_0},\ r^{\mu_1},\ \ldots,\ r^{\mu_{2N-1}})\boldsymbol{a}^m \tag{19}$$

The coordinates of the nth node are denoted by (R,θ_n). Hence, the vector of nodal displacements of the SASE can be given by

$$\hat{\boldsymbol{u}}_p^m = \boldsymbol{T}_t\mathrm{diag}(R^{\mu_0},\ R^{\mu_1},\ \ldots,\ R^{\mu_{2N-1}})\boldsymbol{a}^m \tag{20}$$

where $\boldsymbol{T}_t$ is a transformation matrix. $\hat{\boldsymbol{u}}_p^m$ is defined by $\hat{\boldsymbol{u}}_p^m = \{u_{r,1}\quad u_{\theta,1}\quad u_{r,2}\quad u_{\theta,2}\quad \ldots\quad u_{r,N}\quad u_{\theta,N}\}^{\mathrm{T}}$.

The relationship between $\boldsymbol{a}^m$ and $\hat{\boldsymbol{u}}_p^m$ can be derived from (20), as specified by

$$\boldsymbol{a}^m = \mathrm{diag}(R^{-\mu_0},\ R^{-\mu_1},\ \ldots,\ R^{-\mu_{2N-1}})\boldsymbol{T}_t^{-1}\hat{\boldsymbol{u}}_p^m \tag{21}$$

It should be noted that the number of the chosen expanding terms ($2N$) must be two times of the number of the nodes (N) of the SASE, so that the inverse matrix of $\boldsymbol{T}_t$ can be obtained.

To keep consistent with the global Cartesian coordinate system, a coordinate transformation should be carried out, as specified by

$$\hat{\boldsymbol{u}}_p^m = \boldsymbol{T}_c^{-1}\hat{\boldsymbol{u}}^m,\ \boldsymbol{u}_p^m = \boldsymbol{T}_c^{-1}\boldsymbol{u}^m \tag{22}$$

The coordinate transformation matrix $\boldsymbol{T}_c$ is given by

$$\boldsymbol{T}_c = \mathrm{diag}(\boldsymbol{t}_1,\ \boldsymbol{t}_2,\ \ldots,\ \boldsymbol{t}_N) \tag{23}$$

$$\boldsymbol{t}_n = \begin{bmatrix} \cos\theta_n & -\sin\theta_n \\ \sin\theta_n & \cos\theta_n \end{bmatrix},\quad n = 1,2,\ldots,N \tag{24}$$

Through (19)-(22), the displacement field around the crack tip in the Cartesian coordinate can be given by

$$\boldsymbol{u}^m(x,y) = \boldsymbol{T}_c\boldsymbol{\phi}_u^{\mathrm{T}}(\theta)\mathrm{diag}\left(\left(\frac{r}{R}\right)^{\mu_0}\quad\left(\frac{r}{R}\right)^{\mu_1}\quad\ldots\quad\left(\frac{r}{R}\right)^{\mu_{2N-1}}\right)\boldsymbol{T}_t^{-1}\boldsymbol{T}_c^{-1}\hat{\boldsymbol{u}}^m \tag{25}$$

Thus, the matrix of shape function of the singular element can be given by

$$\boldsymbol{N} = \boldsymbol{T}_c\boldsymbol{\phi}_u^{\mathrm{T}}(\theta)\mathrm{diag}\left(\left(\frac{r}{R}\right)^{\mu_0}\quad\left(\frac{r}{R}\right)^{\mu_1}\quad\ldots\quad\left(\frac{r}{R}\right)^{\mu_{2N-1}}\right)\boldsymbol{T}_t^{-1}\boldsymbol{T}_c^{-1} \tag{26}$$

IV. Finite Element Formulation

The plane dynamic problem represented by (12)-(16) can be solved by the weighted residual method

$$\begin{aligned}&\iint_\Omega \boldsymbol{u}^{*\mathrm{T}}\left(\boldsymbol{L}^{\mathrm{T}}\boldsymbol{\sigma}^m + \boldsymbol{f}^m - \frac{(m+1)(m+2)}{T^2}\rho\boldsymbol{u}^{m+2}\right)\mathrm{d}\Omega \\ &+\int_{\Gamma_u}\boldsymbol{p}^{*\mathrm{T}}(\boldsymbol{u}^m - \bar{\boldsymbol{u}}^m)\mathrm{d}\Gamma - \int_{\Gamma_\sigma}\boldsymbol{u}^{*\mathrm{T}}(\boldsymbol{p}^m - \bar{\boldsymbol{p}}^m)\mathrm{d}\Gamma = 0\end{aligned} \tag{27}$$

Without loss of generality, assuming $\boldsymbol{u}^* = \boldsymbol{0}$ on Γ_u for simplicity and considering (15), (27) can be rewritten as

$$\begin{aligned}&\iint_\Omega \frac{(m+1)(m+2)}{T^2}\rho\boldsymbol{u}^{*\mathrm{T}}\boldsymbol{u}^{m+2}\mathrm{d}\Omega = \\ &\iint_\Omega\left[\boldsymbol{u}^{*\mathrm{T}}\boldsymbol{f}^m - (\boldsymbol{L}\boldsymbol{u}^*)^{\mathrm{T}}\boldsymbol{\sigma}^m\right]\mathrm{d}\Omega + \int_{\Gamma_\sigma}\boldsymbol{u}^{*\mathrm{T}}\bar{\boldsymbol{p}}^m\mathrm{d}\Gamma\end{aligned} \tag{28}$$

In each element, $\boldsymbol{u}^m$ and $\boldsymbol{u}^*$ can be expressed by

$$\boldsymbol{u}^m = \boldsymbol{N}\hat{\boldsymbol{u}}^m,\ \boldsymbol{u}^* = \boldsymbol{N}\hat{\boldsymbol{u}}^* \tag{29}$$

Thus, the finite element formulas can be given by

$$-\frac{(m+1)(m+2)}{T^2}\left[\boldsymbol{M}\right]\left\{\hat{\boldsymbol{u}}\right\}^{m+2} = \left[\boldsymbol{K}\right]\left\{\hat{\boldsymbol{u}}\right\}^m - \left[\hat{\boldsymbol{f}}\right]^m \tag{30}$$

where $\left[\boldsymbol{K}\right]$, $\left[\boldsymbol{M}\right]$ and $\left[\hat{\boldsymbol{f}}\right]^m$ denote stiffness matrix, mass matrix and nodal force vector, respectively. For each element, $\boldsymbol{K}_e$, $\boldsymbol{M}_e$ and $\hat{\boldsymbol{f}}_e^m$ are specified as

$$\boldsymbol{K}_e = \iint_{\Omega_e}\left(\boldsymbol{L}\boldsymbol{N}\right)^{\mathrm{T}}\boldsymbol{D}\left(\boldsymbol{L}\boldsymbol{N}\right)\mathrm{d}x\mathrm{d}y \tag{31}$$

$$\boldsymbol{M}_e = \iint_{\Omega_e}\boldsymbol{N}^{\mathrm{T}}\rho\boldsymbol{N}\mathrm{d}x\mathrm{d}y \tag{32}$$

$$\hat{\boldsymbol{f}}_e^m = \iint_{\Omega_e}\boldsymbol{N}^{\mathrm{T}}\boldsymbol{f}_e^m\mathrm{d}x\mathrm{d}y + \int_{\Gamma_{\sigma,e}}\boldsymbol{N}^{\mathrm{T}}\bar{\boldsymbol{p}}_e^m\mathrm{d}\Gamma_e \tag{33}$$

It should be noted that (33) cannot be applied for SASE. For the SASE subjected to load, $\hat{\boldsymbol{f}}_e^m$ can be derived by introducing special solution to (17).

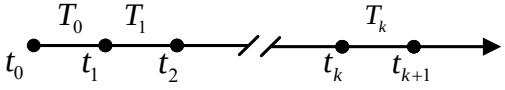

Fig. 3 Initial points and sizes of time intervals

At the first time interval $t \in [t_0, t_1]$, the first two expanding terms can be given by (6), as specified by

$$\hat{\boldsymbol{u}}_0^0 = \hat{\boldsymbol{u}}_0, \ \hat{\boldsymbol{u}}_0^1 = T_0 \hat{\dot{\boldsymbol{u}}}_0 \tag{34}$$

At the kth time interval $t \in [t_k, t_{k+1}]$, the first two expanding terms can be given by using the solutions of the previous time interval, as specified by

$$\hat{\boldsymbol{u}}_k^0 = \sum_{m=0} \hat{\boldsymbol{u}}_{k-1}^m, \ \hat{\boldsymbol{u}}_k^1 = \sum_{m=0} (m+1) \frac{T_k}{T_{k-1}} \hat{\boldsymbol{u}}_{k-1}^{m+1} \tag{35}$$

By solving (30), $\hat{\boldsymbol{u}}_k^m$ ($m > 1$) can be obtained step by step, until the number of expanding terms m is enough. m can be decided automatically by using a convergence criterion

$$\frac{\left\| \hat{\boldsymbol{u}}_k^m \right\|}{\left\| \sum_{j=0}^{m-1} \hat{\boldsymbol{u}}_k^j \right\|} \le \varepsilon \tag{36}$$

where ε is the error bound ($\varepsilon = 10^{-4}$ usually). If the above criterion is satisfied for three consecutive iterations, the computing will be stopped, and the obtained solution is recognized as a convergent one. As long as the nodal displacements are solved, the DSIFs can be obtained directly through the definition, as specified by

$$K_{\mathrm{I}} = \lim_{r \to 0} \sqrt{2\pi r} \sigma_\theta(r, \theta, t) \Big|_{\theta=0} \tag{37}$$

$$K_{\mathrm{II}} = \lim_{r \to 0} \sqrt{2\pi r} \tau_{r\theta}(r, \theta, t) \Big|_{\theta=0} \tag{38}$$

V. Numerical Examples

A. Example 1

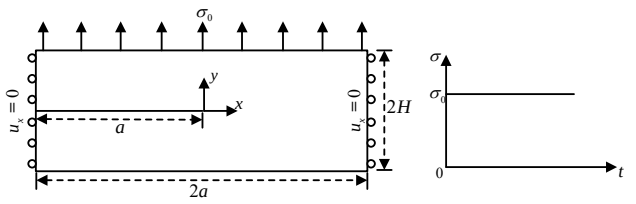

Fig. 4 A semi-infinite plate with an edge crack

As shown in Fig. 4, a semi-infinite plate with an edge crack is considered. The material properties are: mass density $\rho = 8000\ kg/m^3$, Poisson's ratio $v = 0.3$, Young's modulus $E = 210$ GPa .The displacement in the x-direction is $u_x = 0$ at the left edge and the right edge. The length and the height are $2a = 10\ m$ and $2H = 4m$, respectively. The theoretical solution of this problem is available, as specified by

$$K_{\mathrm{I}} = \begin{cases} 0 & 0 < t < t_c \\ \dfrac{2\sigma_0}{1-v} \sqrt{\dfrac{c_d (t - t_c)((1-2v)}{\pi}} & t_c \le t < 3t_c \end{cases} \tag{39}$$

where $t_c = H / c_d$, and c_d is the dilatational wave speed. The mode-I DSIF is normalized by $K_c = \sigma_0 \sqrt{H}$.

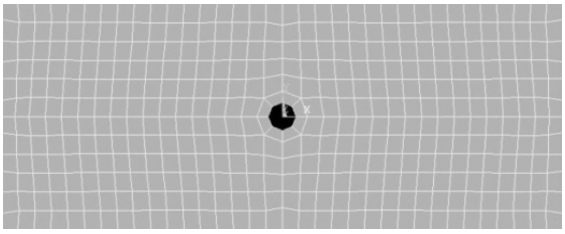

(a) Present method (2742 degrees of freedom)

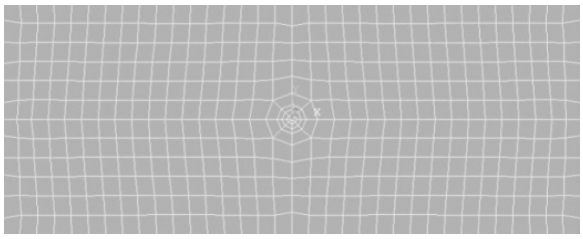

(b) ANSYS (2866 degrees of freedom)

Fig. 5 The finite element meshes of the proposed method and ANSYS

The number of nodes of the SASE is chosen as $N = 17$, and the radius is $R = 0.05a$. Meshes of ANSYS QPE and the present method are shown in Fig. 5. In Fig. 6, numerical solutions of K_{I} obtained through different numerical methods are compared with the exact solution. 100 time steps are chosen arbitrarily in the time domain. In Fig. 7, the numbers of sub-steps in each time step during the calculation are provided.

The impact of the SASE's size on computational accuracy is investigated. A series of SASEs with different radiuses are used to calculate the same problem, while the number of nodes is chosen as $N = 17$. Fig. 8 shows the relative errors compared with the theoretical solution.

The impact of the number of nodes on solving accuracy is also studied. A series of SASEs with different numbers of nodes are used to deal with the same problem, while the radius is chosen as $R = 0.05a$. Fig. 9 shows the relative errors compared with the theoretical solution.

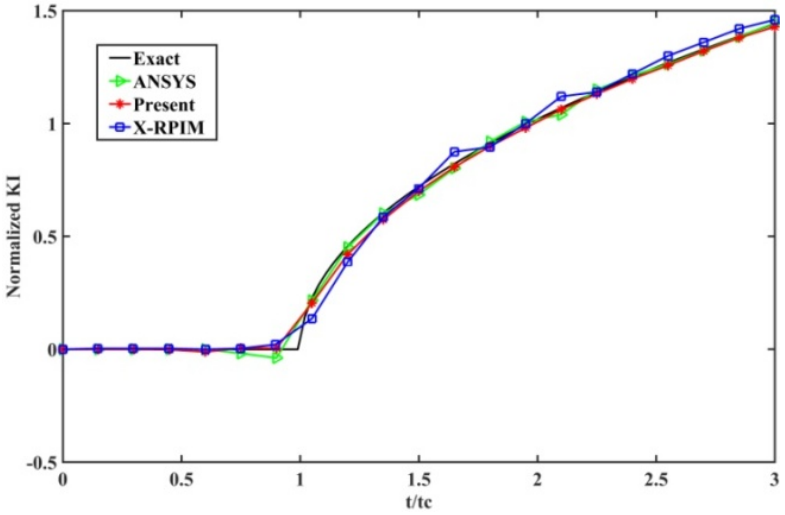

(a) Results

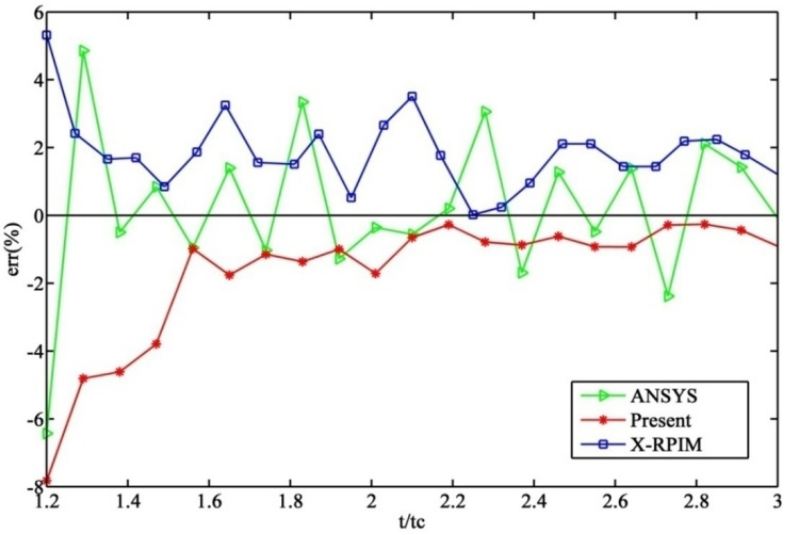

(b) Relative errors

Fig. 6 Results and relative errors of the mode-I DSIF of the edge cracked plate

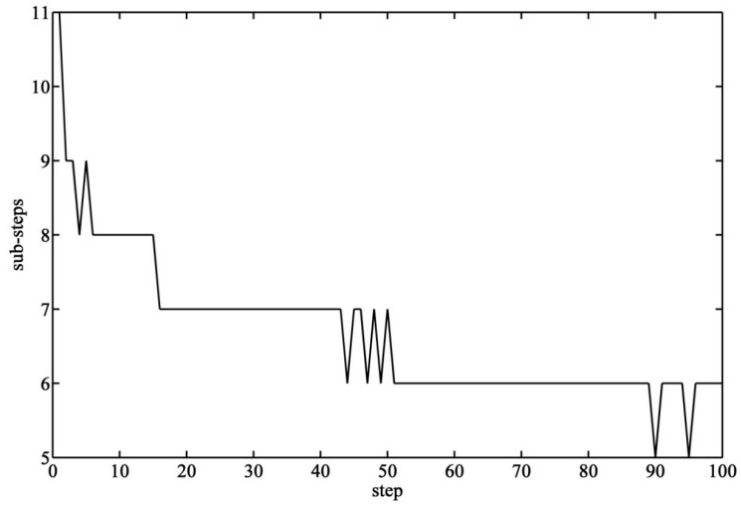

Fig. 7 The number of sub-steps in each step

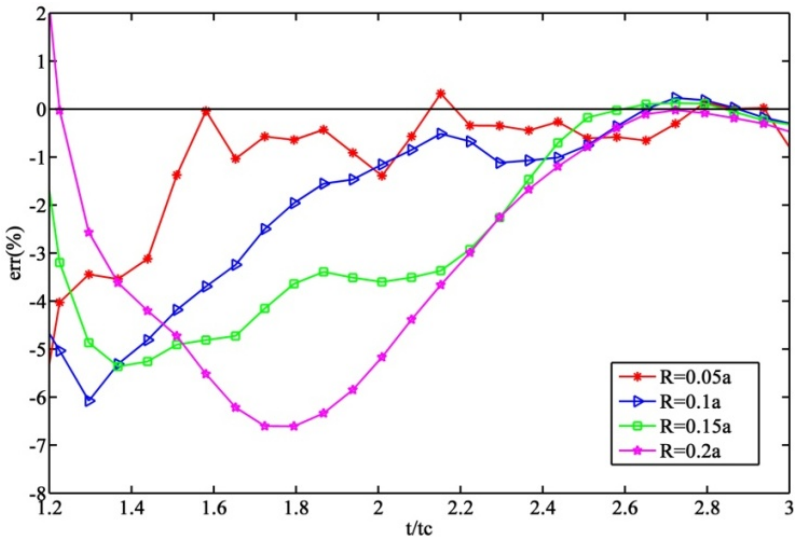

Fig. 8 Relative errors of the mode-I DSIF of the SASEs with different element sizes

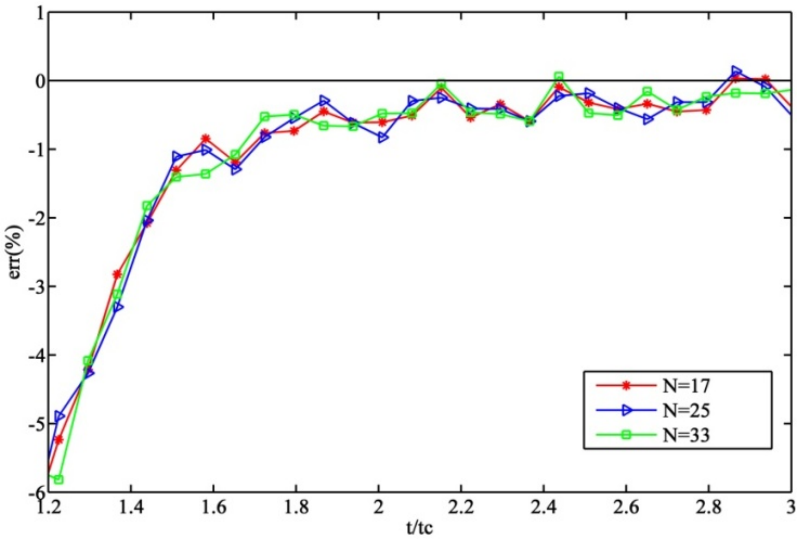

Fig. 9 Relative errors of the mode-I DSIF of the SASEs with different numbers of nodes

B. Example 2

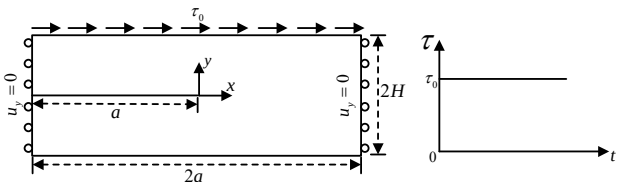

Fig. 10 A semi-infinite plate with an edge crack subject to shear loading

As shown in Fig. 10, a semi-infinite plate with an edge crack is considered. The displacement in the *y*-direction is $u_y = 0$ at the left edge and the right edge. The height is $2H = 4m$. Different lengths $2a = 20\ m,\ 16m,\ 12m$ are chosen. Material properties are: mass density $\rho = 8000\ kg/m^3$, Poisson's ratio $v = 0.3$, Young's modulus $E = 210$ GPa. The theoretical solution of this problem is available, as specified by

$$K_{\mathrm{II}} = \begin{cases} 0 & 0 < t < t_c \\ 2\tau_0 \sqrt{\dfrac{2c_s\left(t - t_c\right)}{\pi\left(1 - v\right)}} & t_c \le t < 3t_c \end{cases} \tag{40}$$

where $t_c = H / c_s$ and c_s is the shear wave speed. The mode-II DSIF is normalized by $K_c = \tau_0 \sqrt{H}$.

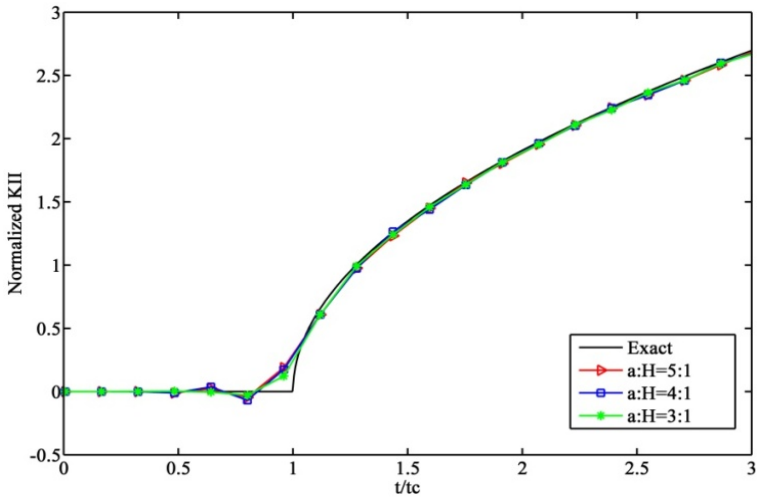

(a) Results

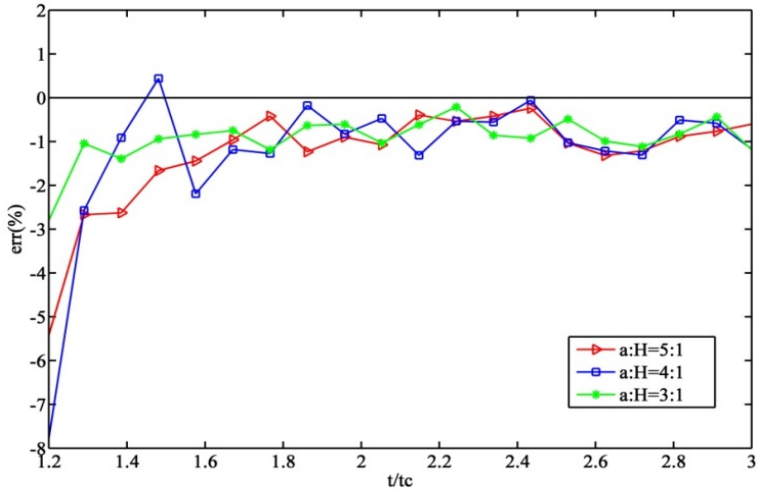

(b) Relative errors

Fig. 11 Results and errors of the mode II DSIFs of an edge crack problem under shear loading

The number of nodes of the SASE is chosen as $N = 17$, and the radius is $R = 0.05a$. Three cases are considered, where different length-width radios are used. In Fig. 11, numerical solutions of K_{II} are compared with the exact solution. Fig. 12 shows the stress distribution in the vicinity of the crack tip.

C. Example 3

As shown in Fig. 13, a semi-infinite plate with an edge crack is considered. The displacement in the *y*-direction is $u_y = 0$ at the top edge and the bottom edge. The geometric dimensions are: $L = 4\ m$, $H = 6\ m$ and $a = 1\ m$. The material properties are: mass density $\rho = 7850\ kg/m^3$, Poisson's ratio $v = 0.25$, Young's modulus $E = 200$ GPa. The prescribed velocity on the boundary is $V_0 = 16.5 m/s$. The analytical solution when $t \le 3t_c$ is available for this problem, where $t_c = a/c_d$, and c_d is the dilatational wave speed. The DSIFs are normalized by $K_c = -EV_0\sqrt{a/\pi}/[2c_d(1-v^2)]$.

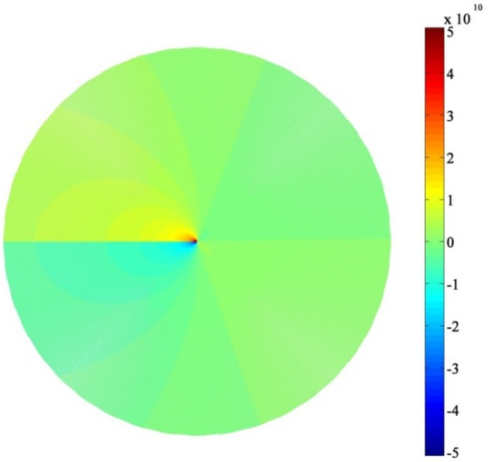

(a) σ_r

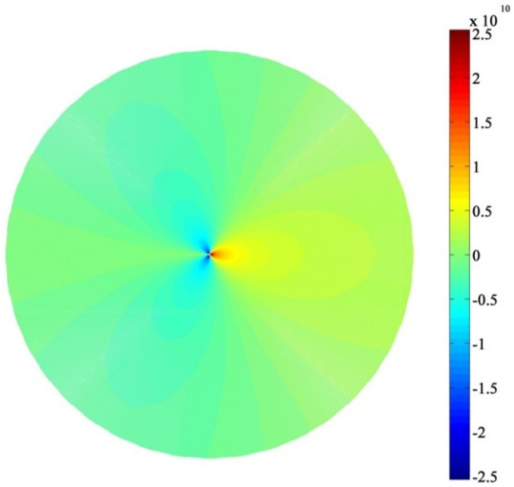

(b) $\tau_{r\theta}$

Fig. 12 The stress distribution near the crack tip ($r \le 0.1R$)

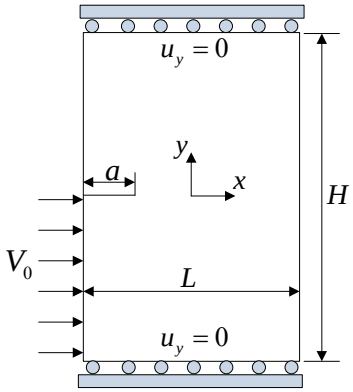

Fig. 13 The geometry and the boundary condition of an edge cracked semi-infinite plate

In Fig. 14 and 15, numerical solutions of DSIFs obtained through different numerical methods are compared with the exact solution. Fig. 16 illustrates the DSIFs obtained by the present method, when different SASEs are used. The number of nodes is chosen as $N = 17$ and the radiuses are $R = 0.25a,\ 0.5a,\ 0.75a$.

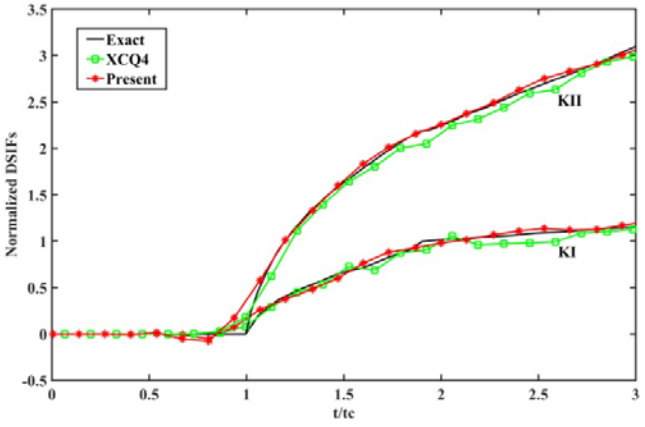

Fig. 14 Results of the DSIFs of the edge crack problem

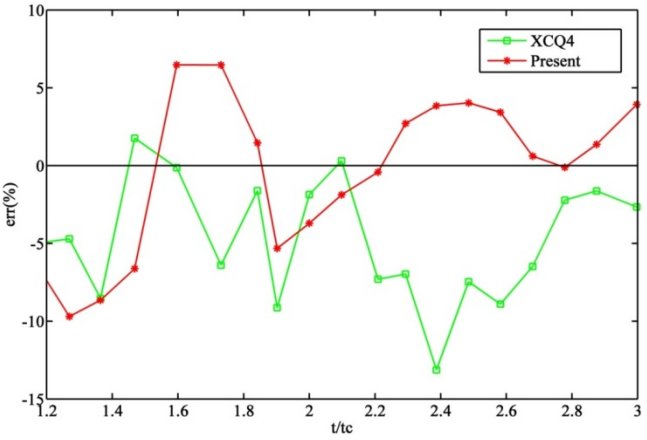

(a) Mode I

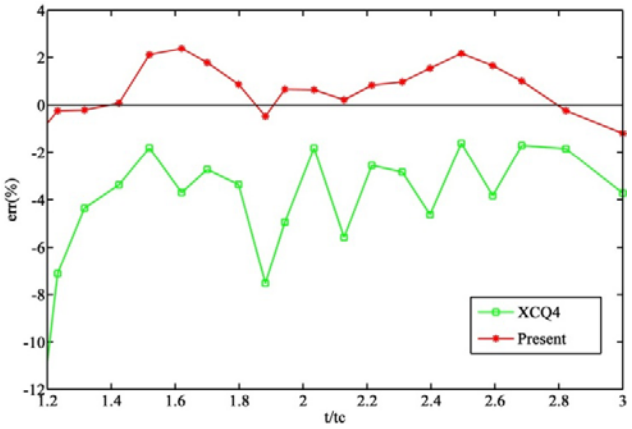

(b) Mode II

Fig. 15 Relative errors of the DSIFs of the edge crack problem compared with the exact solution

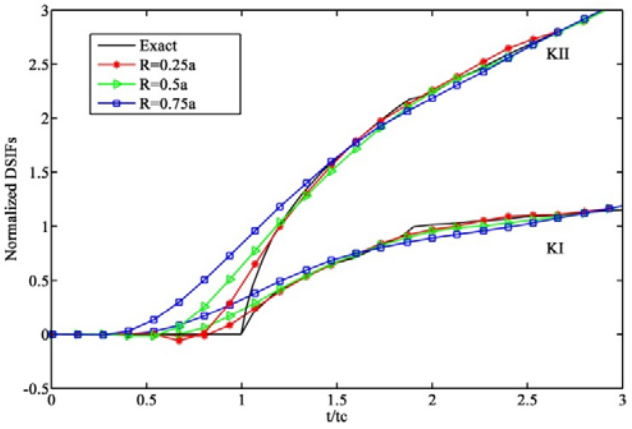

Fig. 16 The DSIFs predicted by the present SASEs with different element sizes

VI. Conclusion

In this study, the SASE is further extended for sharp V-notch problem under dynamic loading condition. The analytical eigenexpanding coefficients around the notch tip are used to represent the fields in the vicinity of notch hence brings higher solving accuracy. The precise time domain expanding

algorithm is adopted to treat the time related problem. Numerical examples show that the proposed method is stable and effective for V-notch problem under dynamic loading condition.

ACKNOWLEDGMENT

The work described in this paper was supported by the National Natural Science Foundation of China (No. 11372065).

REFERENCES

[1] Niu Z, Cheng C, Ye J, Recho N, "A new boundary element approach of modeling singular stress fields of plane V-notch problems," *Int. J. Solids Struct.*, vol. 46, no.16, pp. 2999–3008, Aug. 2009.
[2] Ju SH, "Finite element calculation of stress intensity factors for interface notches," *Comput. Methods Appl. Mech. Eng.*, vol. 199, no. 33-36, pp. 2273–2280, Jul. 2010.
[3] Treifi M, Oyadiji SO, Tsang DKL, "Computation of the stress intensity factors of sharp notched plates by the fractal-like finite element method," *Int. J. Numer. Meth. Eng.*, vol. 77, no. 4, pp. 558–580, Jan. 2009.
[4] Noda NA, Takase Y, "Generalized stress intensity factors of V-shaped notch in a round bar under torsion, tension, and bending," *Eng. Fract. Mech.*, vol. 70, no. 11, pp. 1447–1466, Jul. 2003.
[5] Gross B, Mendelson A, "Plane elastostatic analysis of V-notched plates," *Int. J. Fract.*, vol. 8, no. 3, pp. 267–276, Sept. 1972.
[6] Yi G, Yu T, Bui TQ, Ma C, Hirose S, "SIFs evaluation of sharp V-notched fracture by XFEM and strain energy approach," *Theor. Appl. Fract. Mec.*, vol. 89, pp. 35-44, Jun. 2017.
[7] Yao WA, Hu XF, "A singular finite element on the mixed-mode bimaterial interfacial cracks," *Int. J. Comput. Meth. Eng. Sci. Mech.*, vol. 13, no. 4, pp. 219-226, 2012.
[8] Hu XF, Yao WA, "A new enriched finite element for fatigue crack growth," *Int. J. Fatigue*, vol. 48, pp. 247-256, Mar. 2013.
[9] Yang HT, "A precise algorithm in the time domain to solve the problem of heat transfer," *Numer. Heat Tr. B-Fund.*, vol. 35, no. 2, pp. 243-249, 1999.
[10] Yao WA, Zhong WX, Lim CW, Symplectic Elasticity, World Scientific, 2009.